Broadband transmission losses and time dispersion maps from time-domain numerical simulations in ocean acoustics

Alexis Bottero, Paul Cristini, Dimitri Komatitsch, and Quentin Brissaud

Citation: The Journal of the Acoustical Society of America **144**, EL222 (2018); doi: 10.1121/1.5055787
View online: https://doi.org/10.1121/1.5055787
View Table of Contents: http://asa.scitation.org/toc/jas/144/3
Published by the Acoustical Society of America

Broadband transmission losses and time dispersion maps from time-domain numerical simulations in ocean acoustics

Alexis Bottero,[1,a)] Paul Cristini,[1] Dimitri Komatitsch,[1] and Quentin Brissaud[2]

[1]*Aix Marseille University, CNRS, Centrale Marseille, LMA, Marseille, France*
[2]*Division of Geological and Planetary Sciences, Mail Code 252-21, California Institute of Technology, Pasadena, California 91125, USA*
bottero@lma.cnrs-mrs.fr, cristini@lma.cnrs-mrs.fr, komatitsch@lma.cnrs-mrs.fr, quentinb@gps.caltech.edu

Abstract: In this letter, a procedure for the calculation of transmission loss maps from numerical simulations in the time domain is presented. It can be generalized to arbitrary time sequences and to elastic media and provides an insight into how energy spreads into a complex configuration. In addition, time dispersion maps can be generated. These maps provide additional information on how energy is distributed over time. Transmission loss and time dispersion maps are generated at a negligible additional computational cost. To illustrate the type of transmission loss maps that can be produced by the time-domain method, the problem of the classical two-dimensional upslope wedge with a fluid bottom is addressed. The results obtained are compared to those obtained previously based on a parabolic equation. Then, for the same configuration, maps for an elastic bottom and maps for non-monochromatic signals are computed.

[PEB]
Date Received: April 29, 2018 **Date Accepted:** September 6, 2018

1. Introduction

In underwater acoustics, wave propagation problems typically involve variable geometry and heterogeneous media, which can generate strong signal fluctuations and make the analysis of time signals difficult. Thus, to measure the acoustic energy emitted by a source distributed inside a complex model, acousticians often present results as frequency-dependent transmission loss (TL) curves or TL maps. These maps are traditionally computed in the frequency domain based on the Helmholtz equation.

Two main approaches coexist in the literature to solve this equation in complex environments. The first consists in performing an approximation, usually parabolic, to obtain a solution at a lower computational cost. The second involves discretizing the Helmholtz equation using a full-wave technique (often finite elements), at the cost of a much longer computation time.

This letter presents an alternative approach for the calculation of transmission losses via the wave equation expressed in the time domain. When the source is broadband, it allows one to compute time dispersion maps at no additional computational cost compared to the mono-frequency case. To compute TL maps in the time-domain, one can, in principle, simply store all time signals at all receiver positions and then perform a Fourier transform for each point stored to convert all of them to the frequency domain. However, from a technical point of view this solution is realistic only if the number of receivers is small to moderate because of the amount of storage (in memory or to disk) that the process requires when the number of recording points and/or the number of time steps computed is large to very large. In practice, this limits the generation of frequency-domain results from time-domain simulations to the creation of a small number of TL curves at a limited number of spatial points, preventing the generation of full two-dimensional (2D) TL maps.

The objective of this letter is thus to present an efficient way of creating TL maps from time-domain numerical simulations that avoids the storage of individual time signals. Since the source time signal can be arbitrarily chosen, the TL maps can be evaluated for quasi-monochromatic signals as well as for signals with a wider

[a)]Author to whom correspondence should be addressed.

bandwidth, enabling one to analyze the influence of bandwidth on the distribution of acoustic energy inside the domain. In addition, time dispersion maps can also be calculated on the fly during the simulation, providing an insight into the structure of the received time signals. All these quantities are obtained at a negligible additional numerical cost. It is worth noting that the technique presented is general and can be applied to all methods expressed in the time domain.

Recently, a time-domain spectral-element method (Komatitsch and Tromp, 1999) has been shown to efficiently solve full-wave propagation problems in ocean acoustics (Bottero *et al.*, 2016; Cristini and Komatitsch, 2012). Beyond its capability of handling complex geometries and rheologies accurately, as any finite-element technique, the time-domain spectral-element method runs efficiently on very large computers, exhibiting a computer strong scaling that is almost linear with respect to the number of CPUs or GPUs. This property can lead to a drastic reduction of the duration of numerical simulations compared to some more classical time-domain finite-element techniques. Working in the time domain also allows one to consider arbitrary source time functions and to obtain information on the dispersion of the studied signals.

When used in conjunction with the spectral-element method in the time domain, the implementation of the proposed way of computing TL or time dispersion maps thus has the additional advantage that, contrary to full-wave methods in the frequency domain, the time-domain spectral-element method does not exhibit decreasing performance when increasing the number of processor cores used to perform the calculations. Matrix system solvers (linear solvers) are needed when solving the wave equation in the frequency domain, and their known performance scaling issues on large machines above a thousand processor cores or so (Xu *et al.*, 2013), which is not that high by current high-performance computing standards, implies that some large problems are numerically difficult to handle in the frequency domain, even on the current largest supercomputers.

The letter is organized as follows: Sec. 2 is devoted to the definition of the different physical quantities that we want to study, and to how one can compute them efficiently in a time-domain numerical simulation. Then, in Sec. 3, we provide and discuss some examples of the evaluation of these quantities within the framework of a time-domain spectral-element method. Wave propagation over a fluid and then over an elastic upslope wedge is considered for several source bandwidths. We finally draw some conclusions in Sec. 4.

2. Generalization of the calculation of transmission losses and evaluation of signal time spreading

In this section, we define the different physical quantities that we want to study and show how they can be calculated on-the-fly in a time-domain numerical simulation. These quantities will allow for the evaluation of the transmission losses and of the time structure of signals at all the discrete points of the spatial domain under study. Let us note $u_x(\boldsymbol{x},t)$ and $u_z(\boldsymbol{x},t)$ the horizontal and vertical displacement field, respectively, and $P(\boldsymbol{x},t)$ the pressure field at time t and position $\boldsymbol{x}=(x,z)$. $\dot{u}(\boldsymbol{x},t)=\sqrt{\dot{u}_x(\boldsymbol{x},t)^2+\dot{u}_z(\boldsymbol{x},t)^2}$ is the norm of the particle velocity field. The instantaneous energy per unit volume field in the fluid is given by (Jensen *et al.*, 2011, pp. 11–12),

$$\mathcal{E}(\boldsymbol{x},t)=\frac{1}{2}\rho(\boldsymbol{x})\dot{u}^2(\boldsymbol{x},t)+\frac{1}{2}\frac{P^2(\boldsymbol{x},t)}{\rho(\boldsymbol{x})c^2(\boldsymbol{x})}, \tag{1}$$

where $\rho=1000\,\mathrm{kg\ m^{-3}}$ is the density of water and $c(\boldsymbol{x})$ is the distribution of sound velocity. Likewise, in a linear isotropic solid medium the instantaneous energy is

$$\mathcal{E}(\boldsymbol{x},t)=\frac{1}{2}\rho(\boldsymbol{x})\dot{u}^2(\boldsymbol{x},t)+\frac{1}{2}\sum_{i,j}\epsilon_{ij}(\boldsymbol{x},t)\sigma_{ij}(\boldsymbol{x},t), \tag{2}$$

where $\epsilon(\boldsymbol{x},t)$ and $\sigma(\boldsymbol{x},t)$ are the strain and stress tensors, respectively. Let T_f refer to the duration that is considered, then the integrated energy field reads

$$E(\boldsymbol{x})=\int_0^{T_f}\mathcal{E}(\boldsymbol{x},t)\,\mathrm{d}t. \tag{3}$$

This physical parameter represents the amount of energy received at a given position inside the model at time T_f. It is similar to the radiated seismic energy introduced by Boatwright and Choy (1986) and evaluated from body wave measurements, or to the

T-Phase Energy Flux proposed by Okal (2003) to characterize the energy generated by an earthquake source in the form of a T-wave. Then, knowing the energy E_0 of the emitting source, it is possible to evaluate the transmission losses for time T_f as

$$\mathrm{TL}(\boldsymbol{x}) = -10\log\frac{E(\boldsymbol{x})}{E_0}. \tag{4}$$

Energy is determined by an integral in time, but with the value that we get we have no knowledge of how this energy is distributed within the time interval that we are considering. For a given energy value, time spreading can be very different depending on the propagation path followed by the signal. It is therefore very useful to get such a piece of information. In order to calculate it, we first define the maximum energy field by

$$M(\boldsymbol{x}) = \max_{t<T_f} \mathcal{E}(\boldsymbol{x}, t). \tag{5}$$

This field gives the maximum of the instantaneous energy for each point and provides a way of defining an "effective" time dispersion for a signal as

$$\mathcal{T}(\boldsymbol{x}) = 2\frac{E(\boldsymbol{x})}{M(\boldsymbol{x})}. \tag{6}$$

This quantity is homogeneous to a duration. It represents the duration of the triangle-shaped signal that has the same energy and maximum amplitude as those that we have calculated. It is therefore a measure of the time spreading of the signal. Time-domain numerical simulations provide access to these physical parameters at each time step δt and thus allow for the computation of transmission losses and time dispersion maps on-the-fly during the run at a negligible additional computational cost. In practice, at iteration $i+1$ and position $\boldsymbol{x}$, one can evaluate

$$E_{i+1}(\boldsymbol{x}) = E_i(\boldsymbol{x}) + \mathcal{E}(\boldsymbol{x}, t_{i+1})\delta t, \tag{7}$$

$$M_{i+1}(\boldsymbol{x}) = \max[M_i(\boldsymbol{x}), \mathcal{E}(\boldsymbol{x}, t_{i+1})], \tag{8}$$

$$\mathcal{T}_{i+1}(\boldsymbol{x}) = 2\frac{E_{i+1}(\boldsymbol{x})}{M_{i+1}(\boldsymbol{x})}. \tag{9}$$

Time domain full-wave numerical methods can thus also provide an at-a-glance view of how the acoustic energy emitted by a source is distributed inside a complex heterogeneous model. In Sec. 3, we will show examples of the maps that can be obtained based on the calculation of these physical quantities. In all the examples shown, the final time T_f of the simulations was chosen so that most of the energy produced by the source has left the domain under study.

3. Validation and examples of TL and time dispersion maps

Below we show three sets of results to demonstrate the ability to compute both TL and dispersion maps from time-domain simulations. In the three cases we consider a fluid layer overlying a sloping sea floor. This configuration illustrates several wave propagation phenomena such as mode conversion and mode cutoff due to a varying water column depth. The first problem serves as a validation of the approach by comparing TL maps obtained by a time-domain method to those computed by a reference method in the frequency domain. The second set of results considers an elastic sea floor. It shows the dual effects on the TL maps of pulse bandwidth and shear stiffness in the sea floor. The third set shows dispersion maps for a broadband pulse propagating along and into a fluid sea floor.

3.1 Comparisons of the TL maps with a reference solution

In order to illustrate and validate our approach, we choose to investigate the classical 2D fluid wedge benchmark problem, whose characteristics can be found in Sec. 6.9.2 of Jensen *et al.* (2011). In the context of an attenuating fluid bottom, TL maps for a monochromatic source have already been published there and can thus be used for comparison. These previous results were obtained with a split-step implementation of the Thomson–Chapman parabolic equation using a Greene wide-angle source to initialize the solution. No full-wave Helmholtz solution for this problem is available in the literature.

Let us first generate a TL map from a time-domain numerical simulation for exactly the same configuration. The simulation is based on a time-domain spectral-element method (Komatitsch and Tromp, 1999), which has been shown to efficiently solve full-wave fluid/solid propagation problems in ocean acoustics (Bottero *et al.*,

2016; Cristini and Komatitsch, 2012). In the spectral-element method, viscoacoustic or viscoelastic effects are represented based upon three generalized Zener standard linear solids placed in parallel, with different relaxation times for each, to mimic a constant Q quality factor over the frequency band under study in the simulation (Komatitsch and Tromp, 1999). In order to avoid spurious reflections from the sides of the computational domain, for all configurations the domain is extended up to a range of 20 km and down to a depth of 1 km and equipped with perfectly matched absorbing layers (Xie *et al.*, 2016).

For this work, we define a source time function signal by

$$s(t) = \begin{cases} \frac{A}{2}\left(1 - \cos(\Delta\pi t)\sin(2\pi f_0 t)\right) & \text{if } 0 < t < \frac{2}{\Delta} \\ 0 & \text{else,} \end{cases} \tag{10}$$

where A is the maximum amplitude of the source, f_0 is the dominant frequency of the source signal, and Δ is its bandwidth. This type of time sequence will allow us to control the bandwidth of the emitted signal by changing the value of parameter Δ. Quasi-monochromatic signals that will provide results close to frequency-domain calculations as well as narrowband or broadband signals can be generated. We will thus be able, in Secs. 3.2 and 3.3, to study the influence of the bandwidth on the spreading of acoustic energy inside the computational domain. In addition to a fluid viscoacoustic bottom, we will also consider a solid viscoelastic bottom by adding a shear velocity of $c_s = 600\,\text{m s}^{-1}$ and a shear attenuation coefficient $\alpha_S = 0.5\,\text{dB}\,\lambda_S^{-1}$ to the sediment characteristics.

The first results are shown in Fig. 1, which provides the comparison between a monochromatic TL map [Fig. 1(a)] taken from Jensen *et al.* (2011) and a quasi-monochromatic TL map [Fig. 1(b)] generated from a time-domain full-wave numerical simulation. Typically, the results shown in this letter were obtained in a few seconds using 128 CPU processor cores of a regional cluster, while results for these models using a parabolic equation method are obtained almost instantaneously.

The quasi-monochromatic signal was generated using a bandwidth $\Delta = 0.5$ Hz. We performed several simulations with signals having a smaller bandwidth but did not notice any changes in the TL map. We thus consider this value of the bandwidth as a good approximation of a monochromatic signal for this configuration. Note that this is a fluid only configuration. The two TL maps are very similar. Mode cutoff of the three modes, which exist in the flat part of the model, are recovered almost identically in both cases. The main differences are observed for short ranges. This is not surprising since the parabolic equation, which is used to generate the results of Fig. 1(a), has angular limitations. Moreover, a source with a limited aperture was used, contrary to our simulation, which implements a point source. Therefore the discrepancies between the two TL maps are attributed to the known inaccuracy for steep angles. Nevertheless, interference structures in the water column are very close, except at the end of the wedge where again the grazing angles are steepened because of the varying depth and thus cannot be handled correctly through numerical modeling based on the parabolic equation method which was used. This comparison may be seen as a first answer to the question raised by Buckingham (1992) on the accuracy of TL maps obtained using the parabolic equation for an upslope fluid wedge. Based on the results that we obtain, it can be considered that the accuracy of the parabolic equation is

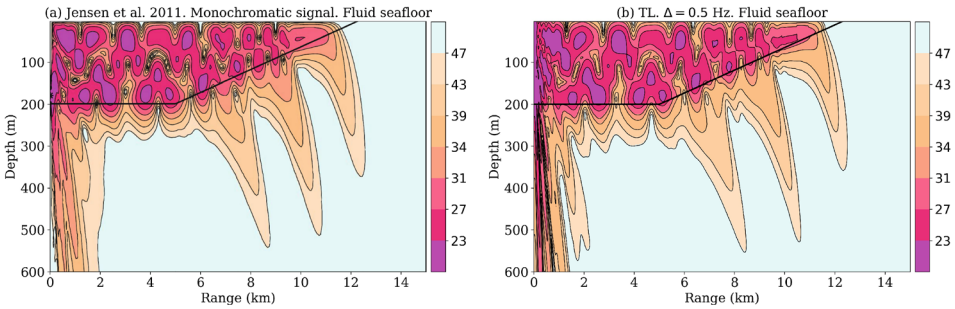

Fig. 1. (Color online) (a) Original TL map, in dB, from Jensen *et al.* (2011, p. 514). (b) TL map from a full-wave time-domain simulation using a quasi-monochromatic source ($f_0 = 25$ Hz, $\Delta = 0.5$ Hz). (a) is reproduced (slightly modified) from Fig. 6.11 of Jensen *et al.* (2011) with permission from Springer. The black line indicates the seabed interface.

good. Moreover, parabolic equation methods have made significant progress in the meantime and should thus compare more favorably nowadays. In particular, wide-angle capabilities that have been developed should at least suppress many of the discrepancies observed in the near field. It should also be noted that if several frequencies are of interest, a simulation is necessary for each frequency considered.

3.2 Effect of pulse bandwidth and sea floor elasticity

Since our numerical method works in the time domain, we can also consider signals with different bandwidths in order to evaluate how this parameter may influence the spreading of energy inside the computational domain. Figure 2(a) represents the TL map for a signal with a bandwidth $\Delta = 8.0$ Hz.

Compared to the monochromatic case [Fig. 1(b)], smoothing of the interference structure is observed in the water column mainly from the beginning of the wedge to its end, the reason being that for each frequency there is a different modal structure, with different grazing angles and therefore different cutoff depths varying continuously with frequency. This smoothing is also observed in the sediment. The complex structure that was observed below the source also disappears.

Adding a shear velocity to the sea floor leads to a very different structure of the leaking of acoustic energy in the bottom [Fig. 2(b)]. The leaking of energy associated to the presence of shear waves is strong and dominant. The associated narrow beams are almost vertical because of the low velocity of shear waves in this configuration. Below the sloping interface, it can be seen that the beams exhibit an interference structure due to the leaking, in this case, of both the shear waves and the propagating modes. This structure is also seen in the near field but, in this case, it is generated by the leaking of evanescent modes. Similar results were presented in Abawi and Porter (2007) (top figure of their Fig. 1). It can also be noted that the leaking of the first mode is strongly affected by the presence of shear waves, as it does not penetrate deep into the sediment. There is much less energy in the water column at the end of the wedge than in the fluid-only configuration. A large amount of energy is captured by the shear waves of the bottom. The structure of the sound field in the sediment suggests that if another interface is considered, i.e., if we consider an elastic layer over a semi-infinite half-space, the presence of shear waves is critical and may generate complex effects because of the potential interaction between these beams and this interface. As in the pure fluid case, increasing the bandwidth [Fig. 2(c)] leads to smoothing of the energy levels mainly in the area of the slope.

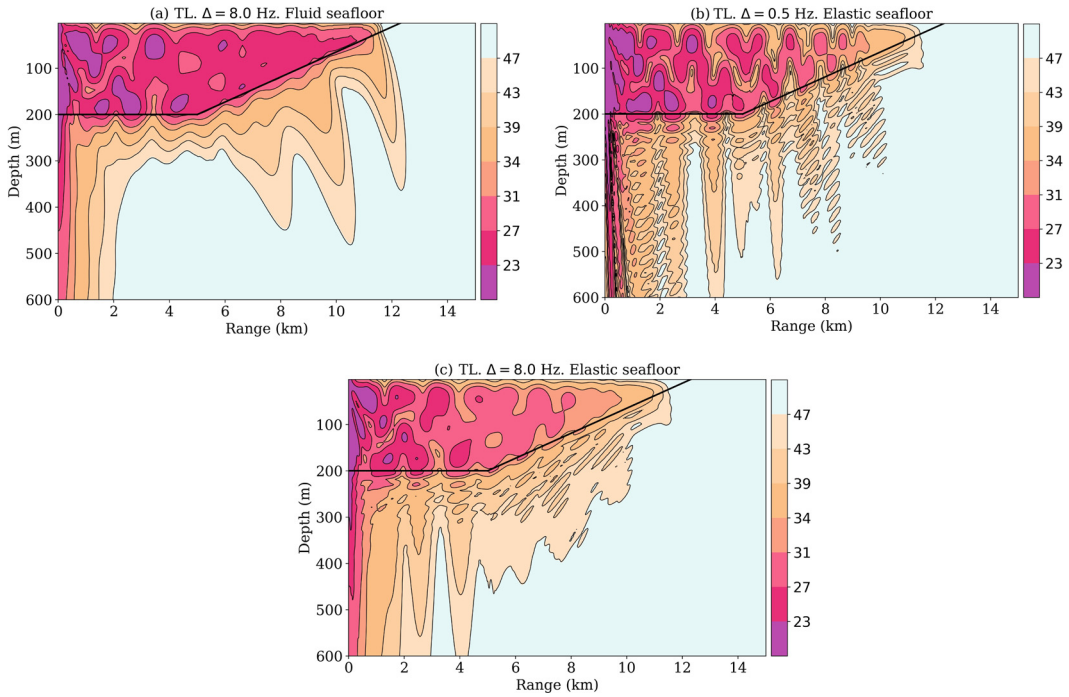

Fig. 2. (Color online) Effect of source bandwidth and bottom elasticity on transmission losses for an upslope wedge. (a) TL map, in dB, for a fluid bottom using a broadband source ($f_0 = 25$ Hz, $\Delta = 8.0$ Hz). (b) TL map, in dB, for an elastic bottom using a quasi-monochromatic source ($f_0 = 25$ Hz, $\Delta = 0.5$ Hz). (c) TL map, in dB, for an elastic bottom using a broadband source ($f_0 = 25$ Hz, $\Delta = 8.0$ Hz).

3.3 Broad bandwidth and time dispersion maps

As mentioned in Sec. 3.2, another type of information can be extracted from time-domain simulations. This piece of information is related to the spreading of energy with time at a receiver location. Indeed, for a given energy level, the time structure of the received signal can be very different and provide additional information on the propagation process that led to this received signal. This is particularly useful, e.g., for T-waves analysis because the time structure of a received signal is different depending on the source mechanism that led to the generation of this signal. In order to illustrate the kind of information that is provided by this type of map, we performed a full-wave time-domain numerical simulation for a fluid bottom and a broadband signal ($f_0 = 25$ Hz, $\Delta = 25.0$ Hz).

Figure 3(a) represents the TL map, and Fig. 3(b) represents the time dispersion map for TL values lower than 43 dB only in order to avoid showing very weak signals. Finally, Fig. 3(c) provides time sequences associated to receivers located at the position of the crosses indicated in Figs. 3(a) and 3(b). These positions were chosen so that the energy level is similar for all positions. The time sequences are arbitrarily shifted for visualization purposes. The time dispersion map exhibits complicated structures reflecting the various time structures that can be generated in this configuration. Signals tend to be more dispersed with range, especially right beneath the sea surface or along the interface with the sea bottom. Nevertheless, at the end of the wedge, at the cutoff depth of mode 1, signals tend to be narrower. This effect is clearly visible in Fig. 3(c).

4. Conclusions and future work

We have presented an efficient procedure to compute transmission losses and time dispersion maps from time-domain full-wave numerical simulations. This procedure allowed us to extend the notion of transmission losses to non-monochromatic signals and to elastic media. Some results using this procedure were obtained for a 2D wedge configuration in ocean acoustics. In the case of a simulation in the frequency domain and for a fluid bottom, these results were compared to results previously obtained using a parabolic equation, showing that both methods give similar results. As a result, our approach can provide solutions for configurations for which using a full-wave numerical method is important because of the complexity of the model. Used in conjunction with a spectral element method in the time domain, this procedure may be used in the future to generate full-wave TL maps for problems that are too large for

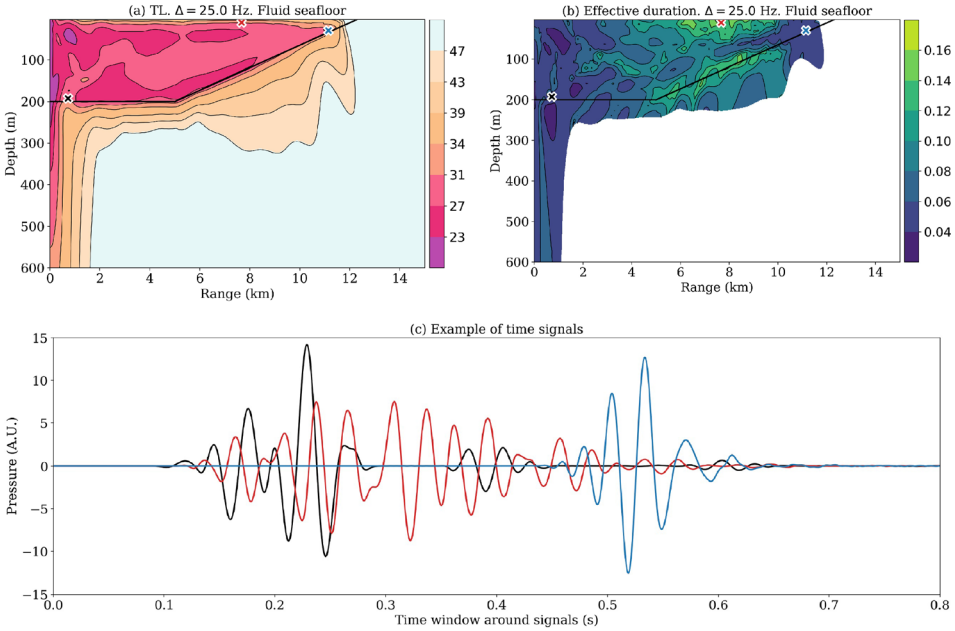

Fig. 3. (Color online) Figure illustrating the use of time dispersion maps. The geometry is the same as in Fig. 1. (a) TL map, in dB, using a broadband source ($f_0 = 25$ Hz, $\Delta = 25.0$ Hz). (b) Associated time dispersion map $\mathcal{T}(\boldsymbol{x})$ (in seconds). This field is shown only for transmission losses that are below 43 dB. (c) Arbitrary time-shifted pressure signals recorded at the positions indicated by the crosses in (a) and (b). The color of each curve corresponds to the color of the respective cross. The wave energy is about the same at the three positions, but the time dispersion is different.

frequency-domain solvers due to their scaling issues. In future work we expect to present results on T-wave propagation or on pile driving, in which this approach may bring new insights into the mechanisms of wave propagation.

Our SPECFEM open source spectral-element software package used in this study is freely available at geodynamics.org; it contains all the tools needed to reproduce the simulations presented in this letter.

Acknowledgments

We are grateful to Jean-Pierre Vilotte, Oleg A. Godin, and Raphaël F. Garcia for fruitful discussion. We also thank associate editor Paul E. Barbone and two anonymous reviewers for useful comments that improved the manuscript. The Ph.D. grant of A.B. was awarded by ENS Paris Saclay, France. This work was granted access to the French HPC resources of TGCC under allocation #gen7165 and #mam0305 and of CINES under allocation #A0020407165 and #A0030410305, both made by GENCI, and of the Aix-Marseille Supercomputing Mesocenter under allocation #b025. We gratefully acknowledge the support of NVIDIA Corporation with the donation of hardware for this research through their Hardware Grant Request program.

References and links

Abawi, A. T., and Porter, M. B. (**2007**). "Propagation in an elastic wedge using the virtual source technique," J. Acoust. Soc. Am. **121**(3), 1374–1382.

Boatwright, J., and Choy, G. L. (**1986**). "Teleseismic estimates of the energy radiated by shallow earthquakes," J. Geophys. Res. **91**(B2), 2095–2112, https://doi.org/10.1029/JB091iB02p02095.

Bottero, A., Cristini, P., Komatitsch, D., and Asch, M. (**2016**). "An axisymmetric time-domain spectral-element method for full-wave simulations: Application to ocean acoustics," J. Acoust. Soc. Am. **140**(5), 3520–3530.

Buckingham, M. J. (**1992**). "Ocean-acoustic propagation models," J. Acoustique **3**, 223–287.

Cristini, P., and Komatitsch, D. (**2012**). "Some illustrative examples of the use of a spectral-element method in ocean acoustics," J. Acoust. Soc. Am. **131**(3), EL229–EL235.

Jensen, F. B., Kuperman, W. A., Porter, M., and Schmidt, H. (**2011**). *Computational Ocean Acoustics*, 2nd ed. (Springer-Verlag, Berlin, Germany), 794 pp.

Komatitsch, D., and Tromp, J. (**1999**). "Introduction to the spectral-element method for 3-D seismic wave propagation," Geophys. J. Int. **139**(3), 806–822.

Okal, E. A. (**2003**). "T waves from the 1998 Papua New Guinea earthquake and its aftershocks: Timing the tsunamigenic slump," Pure Appl. Geophys. **160**(10), 1843–1863.

Xie, Z., Matzen, R., Cristini, P., Komatitsch, D., and Martin, R. (**2016**). "A perfectly matched layer for fluid-solid problems: Application to ocean-acoustics simulations with solid ocean bottoms," J. Acoust. Soc. Am. **140**(1), 165–175.

Xu, R., Liu, B., and Dong, Y. (**2013**). "Scalable hierarchical parallel algorithm for the solution of super large-scale sparse linear equations," J. Appl. Mech. **80**(2), 020901.